IEICE Electronics Express, Vol.16, No.10, 1–6

LETTER

Indoor exclusion zone analysis in a nuclear power plant with wirelessHART application

Jong-Eon Park[1], **Sangwoon Youn**[2], **Jaeyul Choo**[3], **and Hosung Choo**[2a)]

Abstract This article investigates the radiation properties of the wireless devices in nuclear power plants (NPPs) and proposes a new exclusion zone (EZ) with NPP indoor environment. The indoor EZs were affected by the multiple reflections, standing wave, and diffraction depending on the indoor geometry. To accurately analyze the variations between the indoor EZ and free-space EZ, multiple reflection ray tracing, modal analysis of a cylindrical coordinate, and measurements are performed. The results demonstrate that the proposed indoor EZ applied to the NPP environment is more practical and suitable than the EZ in free-space.

Keywords: exclusion zone, field strength, modal decomposition, nuclear power plants

Classification: Electromagnetic theory

1. Introduction

Wireless technologies have become increasingly attractive to nuclear power plants (NPPs) since wireless control and monitoring systems can provide easy connectivity to personnel, sensing systems, and wireless data networks while dramatically reducing the wiring costs [1, 2, 3, 4, 5]. Although the wireless devices are convenient and efficient when operating in NPPs, the corresponding electromagnetic interference (EMI) of devices should be thoroughly verified whether it is below an acceptable level. EMI problems can affect the operation of instrumentation and control (I&C) equipment, especially when the wireless devices are placed in vicinity of system cabinets or cable trays carrying bundles of cables [6, 7, 8]. A simple and partially effective method to reduce EMI events caused by wireless devices is to set up a safety zone around the wireless device so that the system cabinets with I&C equipment cannot be located near the wireless device [9].

The regulation standards for the EMI/radio frequency interference (RFI) in NPPs have been established in several countries, and the most representative regulation is included in the Regulatory Guide 1.180, MIL-STD 461E, EPRI TR-102323, etc. [10, 11, 12]. There are several electromagnetic regulations such as the radiated emission, radiated susceptibility, and exclusion zone (EZ). The EZ is one of the important regulations that must be considered when installing I&C equipment and will be investigated in this work.

The definition of the EZ was introduced in [10], where an allowable radiated electric field was also suggested. These formulas are based on the measurement environment when a broadband horn antenna and a wireless emitter are applied [13]. Two application frequencies were considered with both horizontal and vertical polarizations, and the distance between the two antennas was 0.1 m. The measurement results were obtained from an anechoic chamber, which imitated the free space. However, considering the realistic indoor structure of NPPs, the EZ should be modified in accordance with the indoor environment, such as the arrangement of cabinets, location of the emitter, and dimensions of the room, but there have been no in-depth researches on the EZ according to the indoor structure.

In this article, we study and analyze radiation properties of the wireless devices in the NPP and propose more practical and effective EZ for the NPP indoor environment [14]. The EZ for free space is defined as the minimum separation distance depending on the input power and gain. We then briefly describe the NPP indoor environment to be analyzed and specify the locations of emitters. The electromagnetic simulations are performed, and their electromagnetic power distributions are analyzed. Based on those results, we can obtain the modified EZ including the NPP indoor geometry, which is referred to as "indoor EZ." To accurately analyze the variations between the indoor EZ and free-space EZ, in-depth verifications are performed using the multiple reflection ray tracing, modal analysis [15, 16, 17, 18, 19, 20] in the cylindrical coordinate, and measurements [21, 22]. The results demonstrate that the proposed indoor EZ is more practical and suitable for the NPP environment than the EZ in free-space.

2. Minimum distance estimation in EZ

Minimum distance d in EZ [10] derived from the free space propagation model is

$$d = \frac{\sqrt{30 P_t G_t}}{E} \text{ [m]} \tag{1}$$

where P_t and G_t are the radiated power and antenna gain of the emitter, respectively, and E is the allowable radiated

[1]Metamaterial Electronic Device Research Center, Hongik University, 94 Wausan-ro, Mapo-gu, Seoul 04066, Korea
[2]School of Electronic and Electrical Engineering, Hongik University, 94 Wausan-ro, Mapo-gu, Seoul 04066, Korea
[3]Department of Instrumentation, Control, and Electrical System, Korea Institute of Nuclear Safety, 62 Gwahak-ro, Yuseong-gu, Daejeon 34142, Korea
a) hschoo@hongik.ac.kr

DOI: 10.1587/elex.16.20190204
Received March 28, 2019
Accepted April 4, 2019
Publicized April 16, 2019
Copyedited May 25, 2019

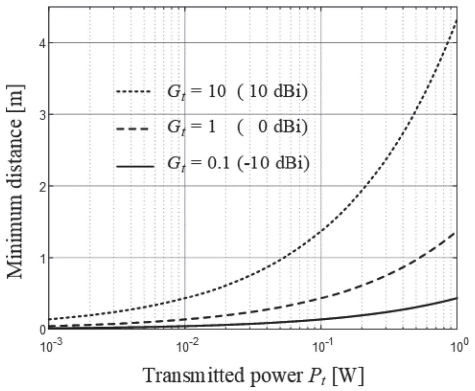

Fig. 1. EZ vs. transmitted power and antenna gain.

Table I. Minimum distance d for typical P_t and G_t.

P_t [W]	d [m]		
	$G_t = 0.1$	$G_t = 1$	$G_t = 10$
0.001	0.01369	0.04330	0.1369
0.01	0.04330	0.1369	0.4330
0.1	0.1369	0.4330	1.369
1	0.433	1.369	4.33

electric field strength of the receiving antenna at the point of installation. The EZ is defined as the allowed minimum distance d from an emitter position. In other words, the safety-related I&C equipment should be located more than the distance d from the emitter to prevent potential EMI problems. Fig. 1 shows the minimum distance d as a function of P_t and G_t when the allowable strength of the E-field is fixed at 4 V/m [10]. As either the antenna gain G_t or radiated power P_t increases, the distance d also does. This indicates that the allowable installation range of the I&C equipment from the emitter is reduced when P_t or G_t increases. Table I shows the distances d for a specific P_t with G_t and corresponds to Fig. 1. The distance d from the definition of the EZ [10] is only valid when the emitter is in free space, but it is not appropriate for an indoor environment that depends on room dimensions or cabinet arrangement. We investigate the phenomena of multiple reflections, standing wave, and diffraction depending on the indoor geometry including walls and large cabinets, and then the modified EZ i.e., the indoor EZ will be obtained as the indoor environment varies.

3. 3D modeling of indoor geometry and field distributions

Fig. 2(a) shows photos of the actual NPP indoor environment, a cable tray, and the I&C equipment and Fig. 2(b) shows a proposed hexahedral indoor geometry, which roughly describes the I&C equipment room in NPPs, to observe electromagnetic scattering characteristics and corresponding indoor EZs. The side represented by l_2 consists of glass windows and metallic frames, and the other five sides (three side walls, floor, and ceiling) are surrounded by concrete walls. The relative permittivities ε_r of the glass

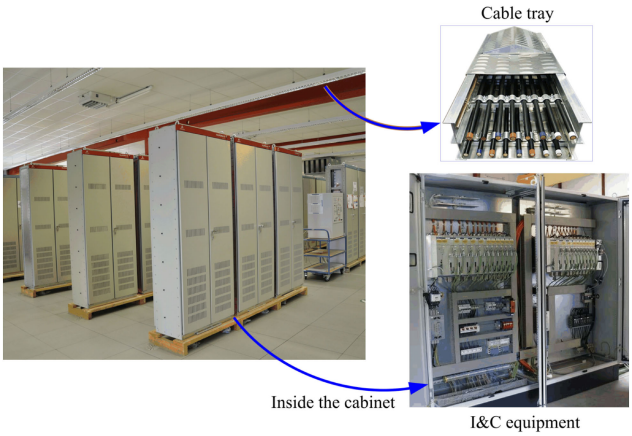

(a)

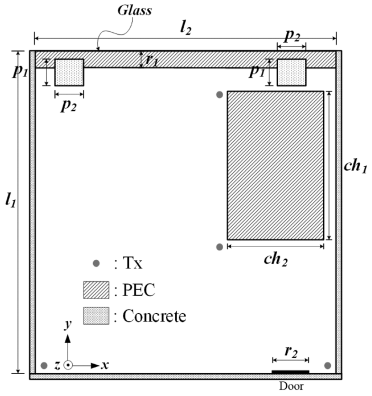

(b)

Fig. 2. (a) Photos of the actual NPP indoor environment, a cable tray, and I&C equipment inside the cabinet and (b) configuration of indoor geometry.

Table II. Dimensions of indoor geometry.

l_1	8.92 m
l_2	8.30 m
p_1	0.74 m
p_2	0.80 m
ch_1	4.13 m
ch_2	2.70 m
r_1	0.44 m
r_2	1.0 m

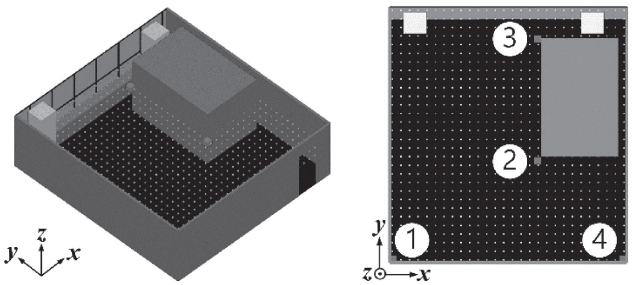

Fig. 3. 3D EM modeling of the indoor geometry (the four square marks indicate transmit antenna locations, and dots are receiver positions).

windows and the concrete walls are 2.4 and $15 - j0.015$, respectively. There are two pillars with $p_1 \times p_2$ in the upper region of the figure, and a large metal cabinet with $ch_1 \times ch_2$ (we assume it to be I&C equipment) is placed in the upper right corner. The height of the room is 2.74 m, and the other specific dimensions are listed in Table II. The modeling does not include detailed cable trays because the volume of those trays is relatively small, and they are located close to the floor or ceiling. The transmitter (Tx) can be mounted in four positions and is indicated by a small gray circle. The transmitter, which emits a signal at 2.4 GHz, is considered to be a measuring equipment using WirelessHART communications [23]. In this case, a vertically polarized dipole antenna is applied, and the antenna is located at 1.4 m from the floor. We also analyze the field distributions for horizontally polarized Tx case and find that the field distributions are also changed by the polarization and radiation pattern of the Tx antenna.

Fig. 3 shows the indoor geometry descriptions using Wireless InSite commercial electromagnetic (EM) simulation software [24], which is useful when indoor propagation characteristics are investigated by a ray-tracing method [25, 26]. The simulation tool is particularly well suited for fast simulation analysis of large indoor spaces. In each case, the transmitter is located at one wavelength away from the wall or metal cabinet. Uniformly distributed dots stand for virtual receiving sensors that measure the EM fields of the room at a height of 1.4 m (receiving sensors are ideal half-wavelength dipole antennas with radiation gain of 0 dBi). The spacings among the adjacent receivers are equally 0.05 m in both the x and y directions.

Fig. 4 describes the EM power strengths for four different Tx locations. The scattered field patterns are dependent on the Tx positions and are non-uniformly distributed with respect to the angle of the radiation, while the field patterns for free space are uniform for the radiation angle. These results indicate that the EZ of the indoor environments should be more carefully investigated since the scattered field distributions are not uniform as the radiation angle varies.

Tx should be mounted at the position with a minimum distance obtained by Eq. (1), however, we have tested various Tx positions. Especially Tx 2 is examined because the position is at the corner angle which is somewhat unique environments compared to other Tx positions. Assuming $G_t = 0.792$ dBi, $P_t = 1.0$ W, and $E = 4$ V/m in Eq. (1), the minimum distance d for the free space is obtained as 1.5 m. The same G_t and P_t are applied in the indoor environment, and then the EZs corresponding to four different Tx locations are obtained as depicted in Fig. 5 as well as free space EZs. The free space EZs, shown as red-dashed lines, are obtained from Eq. (1) and are equidistantly distributed from the Tx positions. The indoor EZs represented by the black area, however, are irregularly distributed due to the scattered E-field in the indoor environment. Key features for the indoor EZs are as follows. (i) The indoor EZ has multiple lobes resulting from multiple reflections and diffractions by the indoor structure. The differences in the number of the lobes in Figs. 5(a) and (b) are due to the varied corner angles of 90°

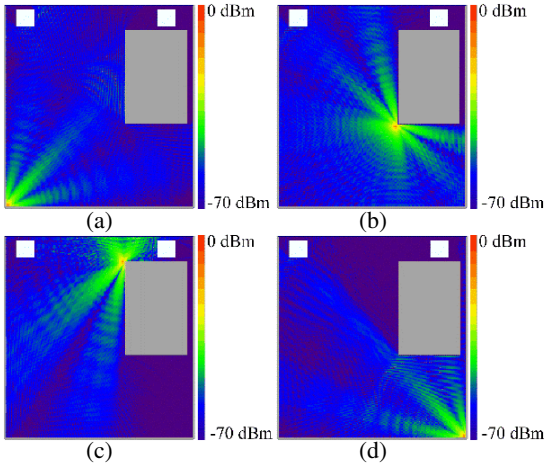

Fig. 4. Simulated power strengths according to the transmitting antenna position. (a) Tx at the lower left in the room (b) Tx at the lower left of the metal cabinet (c) Tx at the upper left of the metal cabinet (d) Tx at the lower right of the room ($P_t = -10$ dBm).

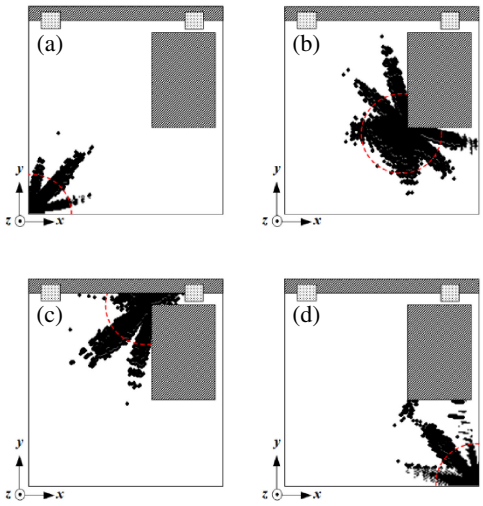

Fig. 5. Indoor EZs and free-space EZs for four different Tx positions.

and 270° between walls, respectively. (ii) The shape and size of lobes for the indoor EZ are formed differently. The middle lobe in Fig. 5(a) is stronger than edge lobes, while the edge lobes in Fig. 5(b) are stronger than the middle lobes. (iii) In the radial direction from the emitter, the EZ appears and disappears repeatedly along the lobes. As shown in Fig. 5(d), along the two lobes near the metallic cabinet, EZ appears repeatedly, and it is due to the standing electromagnetic wave phenomena developed by multiple reflections between the cabinet and the wall. (iv) The field distributions show some variation depending on the height of Tx. The closer Tx is to the ceiling or floor, the weaker field strength and its fluctuation are observed. On the other hand, the field strength and its fluctuation are stronger at the medium height as expected.

It is worthwhile to investigate the propagation of rays at the position farthest from a Tx within the EZ. The Wireless InSite is useful to study the ray propagation phenomena since the software provides multiple ray paths from the emitter to a specific observation position. Fig. 6

Table III. Specific rays' information.

Four strongest rays	Received power strengths and phases
1st (direct ray)	−54.455 dBm and 86.4°
2nd (reflected ray)	−63.087 dBm and 158.4°
3rd (diffracted ray)	−64.075 dBm and −72.0°
4th (diffracted ray)	−64.465 dBm and −100.8°

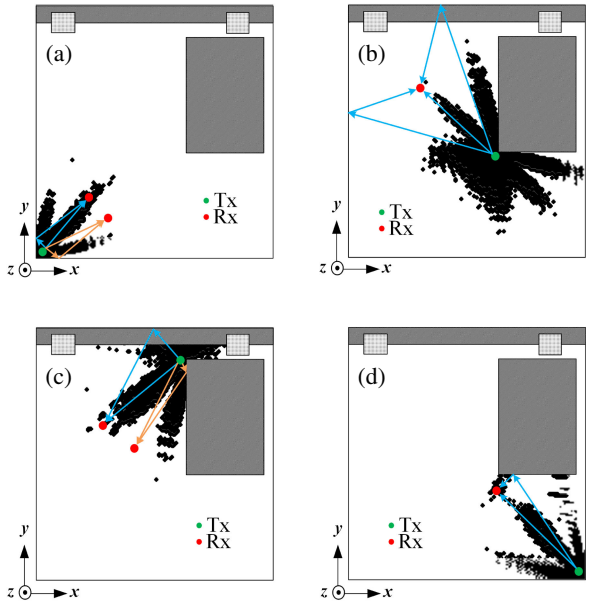

Fig. 6. Ray tracing analyses in accordance with the Tx locations.

shows how the EM rays propagate and reach the farthest EZ position for four different Tx cases. The rays consist of up to six reflected and diffracted rays as well as a direct ray from Tx to Rx. In Figs. 6(a) and (c), the blue and orange sequential arrows indicate the propagating rays reaching specific points inside and outside the EZ, respectively, and the two points are equidistant from the Tx. As shown in Table III, the four strongest rays as represented by the blue lines in Fig. 6(a) are listed, while the other rays are weaker than the listed rays.

In Fig. 6(a), the difference in the electric field strength between the two red points is 5.30 dB. The phase difference of blue rays between the strongest ray path and the sum of the next three strongest rays is 30.57°, which means the rays are constructively superposed. The phase difference of the orange rays under the same condition is 166.26°, which means the rays are destructively superposed. Similarly, the electric field strength difference in Fig. 6(c) is 4.96 dB, and the constructive and destructive phase differences are 71.48° and 176.8°, respectively.

Fig. 7 shows the radiated electric field strength with respect to angle ψ at a distance of 1 m away from the transmitter, when Tx 1 in the inset of Fig. 7(a) is activated. In Fig. 7(a), the line with the circular markers describes the electric field strength obtained by XFdtd EM simulation software [27, 28], when a 2.4 GHz sinusoidal electric field is excited.

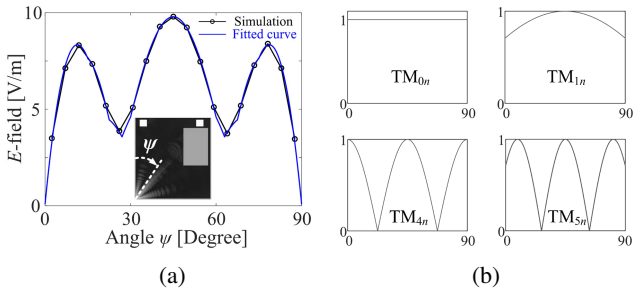

Fig. 7. Radiated electric field strength with respect to angle ψ. (a) Electric field strength and its fitted curve when Tx 1 is activated (Inset). (b) Modal profiles of the TM_{mn} modes for the cylindrical coordinate.

Table IV. Coefficients of the specific modes.

x_0	x_1	x_2	x_3	x_4	x_5	x_6
−341.09	333.09	−92.98	1.6893	2.7278	2.5645	1.0213

$$E_z = x_0 + x_1|\cos\psi + \sin\psi| + \ldots \\ x_2|\cos(2\psi) + \sin(2\psi)| + \ldots \\ x_6|\cos(6\psi) + \sin(6\psi)| \quad (2)$$

The solid line depicts the modal decomposition of the electric fields in terms of angles and is obtained from Eq. (2) of the cylindrical coordinate [29] using a method of least squares [30]. The field distributions of the cylindrical coordinate for the four typical modes ($m = 0$, 1, 4, and 5) are illustrated in Fig. 7(b) to easily understand the modal decomposition. Table IV shows the modal coefficients after fitting a curve. The coefficients x_0, x_1, and x_2 are large, but they cancelled one another out, so that the remaining coefficients contribute to the radiated field strength. The coefficients x_4 and x_5 are relatively greater than x_3 and x_6. In particular, the TM_{4n} mode is dominant since x_4 is the largest coefficient among them. Therefore, at Tx 1 position (90° corner angle, 1 wavelength away from the wall), the TM_{4n} mode contributes the most to the indoor radiation.

The uniform unit cell size on the x, y, and z axes, when executing the XFdtd, is set to 10 mm less than 1/10 of the wavelength of the resonant frequency of 2.4 GHz which is a typical gridding criterion in the finite difference time domain method. The applied frequency is 2.4 GHz, single frequency, and all six sides are assumed to be surrounded by perfectly matched layer-absorbing boundary conditions.

4. Experimental results

Fig. 8(a) shows Tx and Rx antennas and the spectrum analyzer for measurement. Both antennas are the same as a monopole antenna (omnidirectional radiation pattern in xy plane), and a spectrum analyzer MS2720T (Anritsu corporation) is applied to send and receive signals. The cables which connect the analyzer and antennas are long enough in such a way that the analyzer is located away from two antennas and avoids multiple reflections or diffractions by the analyzer. The losses caused by the long cables are

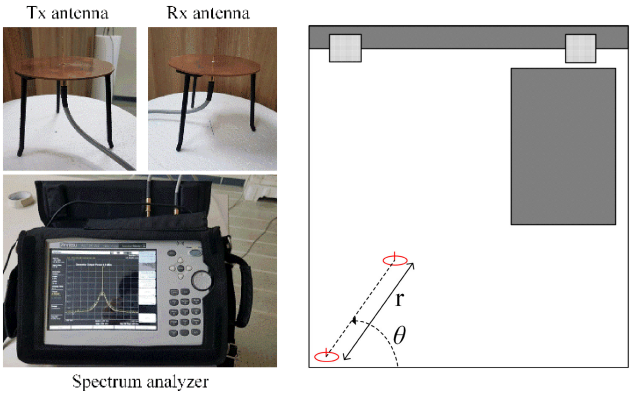

Fig. 8. Measurement setup: (a) transmitting and receiving antennas and spectrum analyzer (b) antenna positions and variable θ.

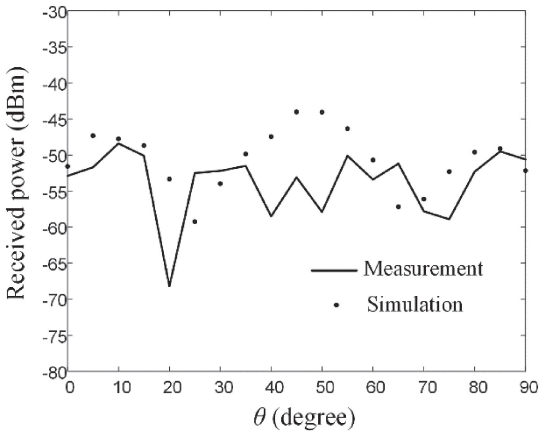

Fig. 9. Measurement and simulation results as a function of angle θ when the Rx location is 1.5 m from the Tx 1.

properly compensated for by using calibration before the measurement. The power level of the transmitted signal is 10 dBm at 2.4 GHz considering the WirelessHART communication application. Fig. 8(b) shows the locations of the Tx and Rx with an angle variable θ. The Tx is fixed at the lower left corner of the NPP room, and the Rx is 1.5 m away from the Tx. Fig. 9 shows the simulated and measured received powers as a function of angle θ. The strong and weak field strengths are observed at similar points, and thus the simulation in the indoor environment agrees with the measurement.

5. Conclusion

We have investigated indoor EZs regarding Tx locations and compared them with free space EZs. The indoor EZs were affected by the multiple reflections, standing wave, and diffraction depending on the indoor geometry. The difference between the strongest and weakest electric field strengths at the same distance from the Tx 1 was observed as 5.3 dB. The EZ patterns at the 90° corner were quite similar to those of the TM_{4n} mode of the cylindrical coordinate. Finally, we compared the simulated and measured power levels at 2 m away from transmitters. Measured fluctuating power levels of around −55 dBm agreed well with the simulation power levels. From this research, we can extensively analyzed indoor EZs for arbitrary indoor environments. In this work, the EZs were obtained only for the vertical polarization. It is necessary to derive the EZs in the same way for the horizontal polarization, and it should therefore be considered in future work.

Acknowledgments

This work was supported in part by the Nuclear Safety Research Program through the Korea Foundation Of Nuclear Safety (KoFONS) using the financial resource granted by the Nuclear Safety and Security Commission (NSSC) of the Republic of Korea (No. 1805006) and in part by the Basic Science Research Program through the National Research Foundation of Korea (NRF) funded by the Ministry of Education (No. 2015R1A6A1A03031833).

References

[1] P. F. Keebler and H. S. Berger: "Managing the use of wireless devices in nuclear power plants," IN Compliance (2011).
[2] J. A. Scerbo, *et al.*: "Safety system augmentation at Russian nuclear power plants," IEEE Trans. Nucl. Sci. **44** (1997) 1084 (DOI: 10.1109/23.603809).
[3] J. Chen, *et al.*: "A thermoelectric energy harvesting system for powering wireless sensors in nuclear power plants," IEEE Trans. Nucl. Sci. **63** (2016) 2738 (DOI: 10.1109/TNS.2016.2606090).
[4] V. Agarwal, *et al.*: "Wireless online position monitoring of manual valve types for plant configuration management in nuclear power plants," IEEE Sensors J. **17** (2017) 311 (DOI: 10.1109/JSEN.2016.2615131).
[5] J.-E. Park, *et al.*: "Electromagnetic scattering of periodic cabinets in nuclear power plants: Parallel polarization," IEEE Access **7** (2019) 16487 (DOI: 10.1109/ACCESS.2019.2893181).
[6] J. Y. Choo, *et al.*: "Transverse electric scattering of open cabinet in nuclear power plants," IEEE Antennas Wireless Propag. Lett. **15** (2016) 1204 (DOI: 10.1109/LAWP.2015.2501368).
[7] H. M. Hashemian, *et al.*: "Methods for testing nuclear power plant cables," IEEE Instrum. Meas. Mag. **16** (2013) 31 (DOI: 10.1109/MIM.2013.6616289).
[8] Y. Tian, *et al.*: "Third-order channel propagation model-based indoor adaptive localization algorithm for wireless sensor networks," IEEE Antennas Wireless Propag. Lett. **12** (2013) 1578 (DOI: 10.1109/LAWP.2013.2293578).
[9] J. Li, *et al.*: "Influence of DC supply systems on unplanned reactor trips in nuclear power plants," Tsinghua Sci. Technol. **6** (2001) 84.
[10] Nuclear Regulatory Commission: "Guidelines for evaluating electromagnetic and radio-frequency interference in safety-related instrumentation," Regulatory Guide 1.180, Office of nuclear regulatory research (2003).
[11] Department of Defense: "Requirements for the control of electromagnetic interference characteristics of subsystems and equipment," MIL-STD-461G (2010).
[12] Electric Power Research Institute: "Guidelines for electromagnetic interference testing of power plant equipment," Revision 3 to EPRI TR-102323 (2004).
[13] S.-H. Ye, *et al.*: "Verification of electromagnetic effects from wireless devices in operating nuclear power plants," Nucl. Eng. Technol. **47** (2015) 729 (DOI: 10.1016/j.net.2015.06.014).
[14] L. K. Singh, *et al.*: "Early prediction of software reliability: A case study with a nuclear power plant system," Computer **49** (2016) 52 (DOI: 10.1109/MC.2016.15).
[15] J.-E. Park, *et al.*: "Analysis of deep-subwavelength Au and Ag slit transmittances at terahertz frequencies," J. Opt. Soc. Am. B **33** (2016) 1355 (DOI: 10.1364/JOSAB.33.001355).
[16] Ş. E. Kocabaş, *et al.*: "Modal analysis and coupling in metal-

insulator-metal waveguides," Phys. Rev. B **79** (2009) 035120 (DOI: 10.1103/PhysRevB.79.035120).
[17] B. Sturman, *et al.*: "Theory of extraordinary light transmission through arrays of subwavelength slits," Phys. Rev. B **77** (2008) 075106 (DOI: 10.1103/PhysRevB.77.075106).
[18] Y.-K. Hue and F. L. Teixeira: "Numerical mode-matching method for tilted-coil antennas in cylindrically layered anisotropic media with multiple horizontal beds," IEEE Trans. Geosci. Remote Sens. **45** (2007) 2451 (DOI: 10.1109/TGRS.2007.900981).
[19] W. C. Chew: *Waves and Fields in Inhomogeneous Media* (Wiley, New York, 1999) 327.
[20] A. Wexler: "Solution of waveguide discontinuities by modal analysis," IEEE Trans. Microw. Theory Techn. **15** (1967) 508 (DOI: 10.1109/TMTT.1967.1126521).
[21] C.-F. Yang, *et al.*: "A ray-tracing method for modeling indoor wave propagation and penetration," IEEE Trans. Antennas Propag. **46** (1998) 907 (DOI: 10.1109/8.686780).
[22] K. A. Remley, *et al.*: "Improving the accuracy of ray-tracing techniques for indoor propagation modeling," IEEE Trans. Veh. Technol. **49** (2000) 2350 (DOI: 10.1109/25.901903).
[23] International Electrotechnical Commission: "Industrial networks - Wireless communication network and communication profiles - WirelessHART," IEC 62591 (2016).
[24] Remcom: Wireless InSite (2018) http://www.remcom.com/wireless-insite.
[25] H. Shin, *et al.*: "Analysis of radar cross section of a battleship equipped with an integrated mast module based on PO and PTD," J. Electromagn. Eng. Sci. **17** (2017) 238 (DOI: 10.26866/jees.2017.17.4.238).
[26] C. Kim and Y. B. Park: "Prediction of electromagnetic wave propagation in space environments based on geometrical optics," J. Electromagn. Eng. Sci. **17** (2017) 165 (DOI: 10.5515/JKIEES.2017.17.3.165).
[27] Remcom: XFdtd 3D electromagnetic simulation software (2018) https://www.remcom.com.
[28] Y. Wang, *et al.*: "A hybrid technique based on combining ray tracing and FDTD methods for site-specific modeling of indoor radio wave propagation," IEEE Trans. Antennas Propag. **48** (2000) 743 (DOI: 10.1109/8.855493).
[29] C. A. Balanis: *Advanced Engineering Electromagnetics* (Wiley, New York, 1989) 3rd ed. 492.
[30] W. Cheney and D. Kincaid: *Numerical Mathematics and Computing* (Brooks Cole, Belmont, 2012) 5th ed. 523.